A Deep Ensemble Encoder Network Method for Improved Polygenic Risk Score Prediction

Okan Bilge Ozdemir[1], Ruining Chen[1], Ruowang Li[1]

1. Cedars-Sinai Medical Center, Computational Biology Department, Los Angeles, CA, USA

Abstract

Genome-wide association studies (GWAS) of various heritable human traits and diseases have identified numerous associated single nucleotide polymorphisms (SNPs), most of which have small or modest effects. Polygenic risk scores (PRS) aim to better estimate individuals' genetic predisposition by aggregating the effects of multiple SNPs from GWAS. However, current PRS is designed to capture only simple linear genetic effects across the genome, limiting their ability to fully account for the complex polygenic architecture. To address this, we propose DeepEnsembleEncodeNet (DEEN), a new method that ensembles autoencoders and fully connected neural networks (FCNNs) to better identify and model linear and non-linear SNP effects across different genomic regions, improving its ability to predict disease risks. To demonstrate DEEN's performance, we optimized the model across binary and continuous traits from the UK Biobank (UKBB). Model evaluation on the held-out UKBB testing dataset, as well as the independent All of Us (AoU) dataset, showed improved prediction and risk stratification, consistently outperforming other methods.

Introduction

Many human traits and diseases are highly heritable, reflecting the important influences of the underlying genetics[1–5]. To date, GWAS have identified over 70,000 SNP associations spanning a wide range of human traits and diseases[6–11]. Effective leveraging of these genotype-phenotype correlations to construct genetic risk prediction models holds substantial clinical promise by enabling early and stable risk predictions[12–14]. However, individual SNPs typically account for only a fraction of phenotype variability. The recent development of polygenic risk score[15–17] (PRS), which aggregates univariate effects from many genetic loci identified through GWAS, has shown improved performance in predicting and stratifying genetic susceptibilities in large populations[18–20]. Nevertheless, existing PRS methodologies are constrained by inflexible underlying assumptions of genetic data that limit their ability to fully capture the predictive signals[21].

Broadly speaking, existing PRS methodologies, such as pruning and thresholding[22–24], Lasso regularized regressions[25] or Bayesian methods[26–30], vary in their approaches to estimate the effects of individual SNPs. Nonetheless, these methodologies often share similar fundamental assumptions. Current PRS models primarily focus on the effects of univariate SNPs and their linear additive aggregations, thus not allowing potential non-linear effects to be captured[31,32]. In addition, they also generally assume uniform signal distributions across the genome, as reflected by fixed modeling parameters, e.g., a single λ in Lasso, applied to all SNPs. Furthermore, given the high dimensionality and sparsity of genetic data, many PRS approaches utilize dimensionality reduction or variable selection techniques to improve the signal-to-noise ratio in the input feature space. However, dimensionality reduction typically occurs concurrently with classification or

regression in the supervised learning setting. Separating these tasks could yield more efficient methods, as better strategies exist for each task independently.

Autoencoders are highly efficient in data dimensionality reduction, making them particularly valuable in areas such as imaging and natural language processing[33–37]. They function by learning a lower-dimensional representation of the data that can minimize data reconstruction error, effectively capturing key features while discarding noise and redundant information. On the other hand, fully connected neural networks (FCNN) are considered state-of-the-art in predictive modeling due to their ability to process complex, high-dimensional data and learn complex patterns[38–41]. The architecture of FCNN allows for the learning of hierarchical representations of underlying data, improving tasks such as regression and classification. However, despite their respective strengths, autoencoders and FCNNs have not been utilized in ensemble learning to integrate latent representation learning with predictive modeling for improving genetic risk prediction models[42–44].

In this study, we propose a novel method, DeepEnsembleEncodeNet (DEEN), which utilizes an autoencoder for learning latent genetic feature representations coupled with a FCNN for constructing predictive models. DEEN disentangles genetic data dimensionality reduction and prediction model construction into separate modules, allowing optimal learning for each task. The autoencoder module extracts a lower-dimensional latent representation of the genetic data that can capture both linear and non-linear relationships among the SNPs. Subsequently, the FCNN further enables learning of non-linear effects as well as differential variable weighting across the genome, providing a substantially more flexible framework for capturing diverse genetic effects in constructing genetic risk prediction models. We optimized DEEN using binary diseases, type 2 diabetes (T2D) and hypertension, and continuous phenotypes, body mass index(BMI), cholesterol, high-density lipoprotein (HDL), low-density lipoprotein(LDL), from the UKBB dataset[45]. We then evaluated its performance internally on separate held-out UKBB testing datasets and externally on the independent All of Us (AoU) dataset. Results from these analyses demonstrate that DEEN achieved superior predictive performance for all phenotypes compared to existing methods. Moreover, the DEEN model significantly improved the stratification of various risk groups, demonstrating its potential for clinical utility.

Results

Overview of the DEEN algorithm

The DEEN algorithm comprises of three main components (Figure 1). Unsupervised autoencoder for learning latent representations: In the initial stage, DEEN employs an unsupervised autoencoder to derive lower-dimensional latent representations of the input SNPs for each chromosome. This approach leverages the expected correlations among the SNPs, such as those arising from linkage disequilibrium, to generate features that encode the independent variations among the SNPs. Each chromosome is modeled separately due to the minimal correlations expected across chromosomes. Concatenation of Latent Representations: In the second stage, the latent representations obtained from each chromosome are concatenated to form a combined feature set for predictive modeling. Supervised learning using an FCNN: The final stage involves using a supervised FCNN to model the chromosome-specific autoencoders. The FCNN can capture both linear and non-linear relationships among the input features, thus offering a broadened search space for identifying the optimal model. Notably, the FCNN

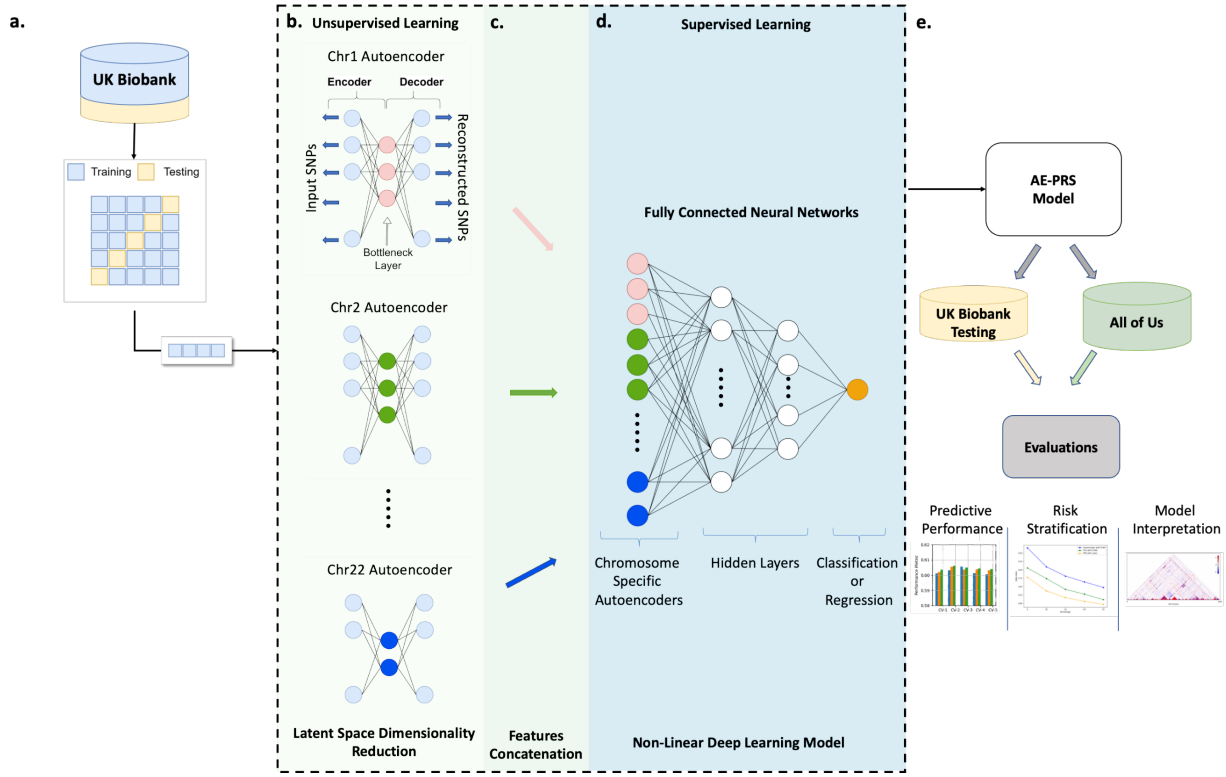

Figure 1 **Overview of the study design and the DEEN algorithm** ***a****. The UKBB dataset is divided into 5 equal parts for each phenotype. In each iteration, one fold is used as the test set, while the remaining 4 folds are used for training. This process is repeated 5 times, with each fold used exactly once as the test set.* ***b****. Unsupervised latent space dimensionality reduction is performed using autoencoders with only genetic data.* ***c****. A single representation matrix for each patient is created by concatenating the latent space matrices obtained from the autoencoders.* ***d****. Supervised classification/regression with FCNN is carried out using the representation matrices obtained in part c and the phenotype data.* ***e****. Performance evaluations are conducted on the UKBB and All of Us datasets.*

inherently allows differential impacts of various genomic regions on the final prediction, thereby providing a more accurate representation of the underlying genetic effects. To assess the model, DEEN was trained using 5-fold cross-validation on the UKBB dataset. The trained models were subsequently evaluated for their predictive performance, risk stratification, and interpretation using the independent All of Us dataset.

Evaluations in UKBB and AoU Datasets

We optimized DEEN on UKBB training data for two binary phenotypes—hypertension and T2D as well as four continuous phenotypes: BMI, cholesterol, LDL, and HDL. The models' predictive performance was assessed on the held-out UKBB testing data. We also evaluated existing PRS methods, including the summary-statistics PRS-CS [26], and Lasso (as implemented in bigsnpr) using individual-level data[46], and an alternative ML method, PCA-FCNN, on the same datasets.

Figure 2a shows that DEEN achieved higher AUC scores for the two binary diseases compared to other evaluated PRS methods. In the UKBB dataset, DEEN's AUC for T2D is 3.01% higher than the Lasso, and 1.49% higher for hypertension. Compared to PRS-CS, DEEN's AUC improvement is 7.99% for Hypertension and 9.29% for T2D. Compared to PCA-FCNN, the improvement is 0.47% for Hypertension and 1.22% for T2D.

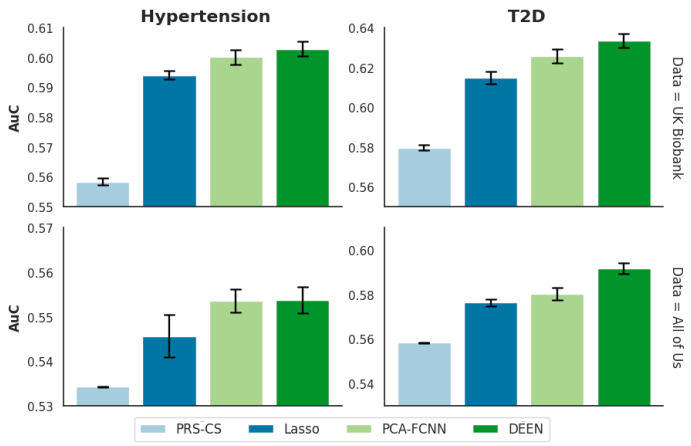

(a)

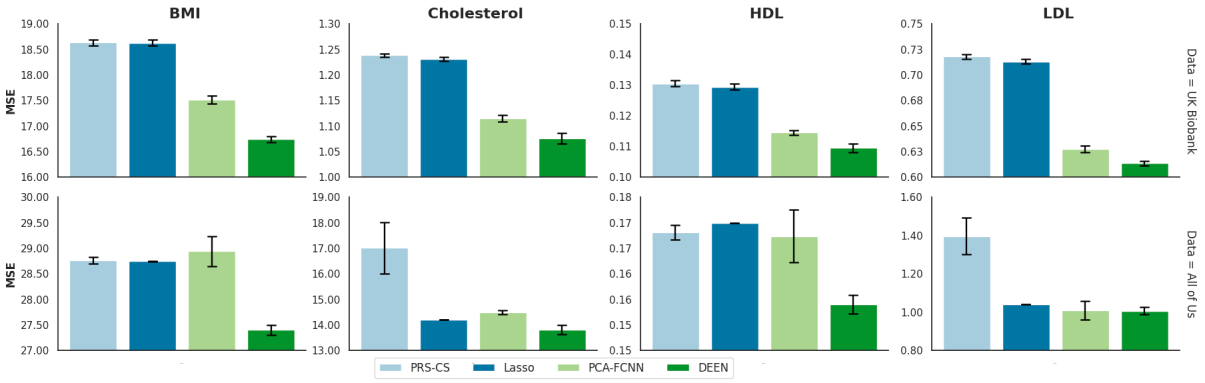

(b)

Figure 2 *Predictive performances of DEEN and existing PRS methods on binary diseases and continuous traits in UKBB and AoU. The models compared in the figures are DEEN (green), PCA-FCNN (light green), Lasso (dark blue) and PRS-CS (light blue).* ***a.*** *AuC values for different prediction models applied to Hypertension and T2D using data from the UK Biobank and All of Us datasets. The top row shows the results for the UK Biobank dataset, with Hypertension on the left and T2D on the right. The bottom row shows the results for the All of Us dataset in the same order.* ***b.*** *MSE values of the different prediction models for continuous phenotypes: BMI, Cholesterol, HDL and LDL phenotypes respectively. The top row shows the results for the UK Biobank dataset and in the bottom row, the results for the All Of Us dataset are shown in the same order as the given phenotypes.*

Beyond predictive performance, we also evaluated the models' ability to stratify risk for binary diseases, aligning more closely with their clinical utility. The analysis was performed by comparing the odds ratio enrichment of cases between high-risk and low-risk groups. Different risk quantiles (top 5%, 10%, 15%, 20%, and 25%) were used to select the high-risk group while the low-risk group was kept constant (bottom 5%). DEEN outperformed existing PRS approaches and PCA-FCNN in stratifying the two risk groups(Figure 3). For T2D, DEEN improved the odds ratio enrichment by an average of 25.99% compared to Lasso, 93.68% compared to PRS-CS, and 24.02% compared to PCA-FCNN. For hypertension, the respective average improvements are 10.46%, 77.40%, and 3.74%.

Figure 2b shows the performance evaluation of the models for continuous phenotypes. Consistent with the binary disease results, DEEN achieved lower mean squared error (MSE) for all continuous phenotypes. For BMI, DEEN reduced the MSE by 4.41% compared to PCA-FCNN, 10.11% compared to Lasso, and 10.14% compared to PRS-CS. For cholesterol, the MSE reduction

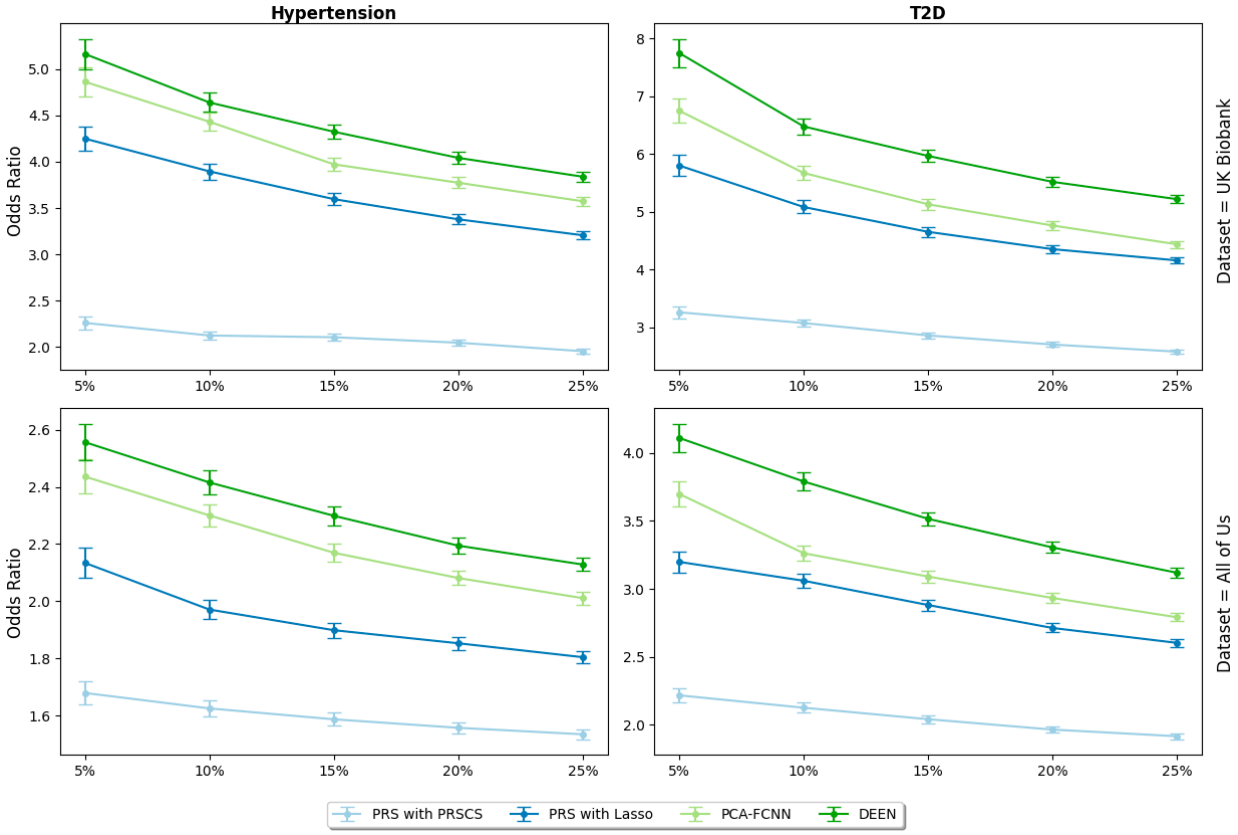

Figure 3 *DEEN has improved risk stratification for T2D and Hypertension for the best-performing models. The models compared are DEEN (green), PCA-FCNN (light green), Lasso (dark blue), and PRSCS (light blue). The x-axis represents different percentage thresholds (5%, 10%, 15%, 20%, 25%) for selecting the high-risk group, and the y-axis shows the odds ratios enrichment of cases between the high- and low-risk groups for each threshold. 95% confidence intervals are shown for each odds ratio. Results for UKBB are displayed in the top row, and for AoU are on the bottom row.*

is 3.59%, 12.65%, and 13.18%, respectively. HDL showed the largest MSE reduction, with improvements of 4.44%, 15.40%, and 16.11%. Lastly, for LDL, the MSE improvement is 2.24%, 13.98%, and 14.54%, respectively.

External validation on the AoU dataset is shown in the bottom panels of Figure 2 and Figure 3. While the prediction AUC decreased on average for binary phenotypes across all methods, the proposed DEEN procedure still achieved the best results for all phenotypes. In addition, the odds-ratio analysis demonstrated that the improvement in stratifying risk groups remained stable. In each case, the DEEN method outperforms the other methods.

For continuous phenotypes, the DEEN model applied to the AoU dataset continued to outperform other methods, similar to the results obtained with the UKBB dataset. In contrast, the performance of other methods varied. Lasso outperformed PCA-FCNN for BMI and Cholesterol, while PRS-CS outperformed PCA-FCNN for BMI and Lasso for HDL.

To further investigate the improved performance of DEEN compared to the best-performing PRS method, Lasso PRS, SNPs' contributions to the final predictions were compared using model outputs from the T2D analysis (Figure 4). As DEEN disentangles dimensionality reduction and predictive modeling, most SNPs were retained by the model as they may contribute to either reconstructing the genetic features or predicting the outcomes. In contrast, around 90% of the SNPs have zero coefficients in the lasso model as the model only retains SNPs that are both

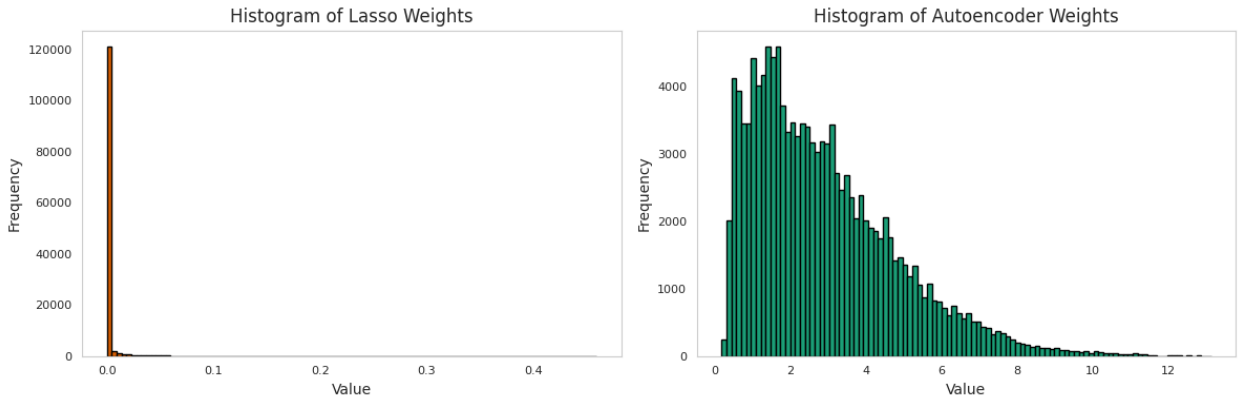

Figure 4 *Comparison of SNP contributions between autoencoder and Lasso. Each histogram displays the frequency distribution of respective SNP weight values of Lasso regression (left) and the autoencoder model (right) for T2D disease.*

correlated with the outcome and representative of the feature space. Therefore, DEEN comparatively utilizes more SNPs when constructing the prediction models. Similar results were observed for other chromosomes and diseases.

The autoencoder can also capture both local and distal relationships among the SNPs. Using autoencoder outputs from the same T2D analysis, Figure 5a shows the Pearson correlations among the SNPs based on their estimated feature weights in the autoencoder model. Since the SNPs are organized according to their physical locations across the chromosomes, SNPs in proximal distances showed the highest correlations, reflecting local linkage disequilibrium. However, the autoencoder model also captured correlations among SNPs in distant regions, which are often not modeled by existing PRS methods.

Additionally, the nodes in the bottleneck layer can differentially model the SNPs. Comparing the SNPs' weights connected to each node in the bottleneck layer revealed distinct groups of nodes with similar SNP connections, indicating that the autoencoder has distinct structures modeling different parts of the genome (Figure 5b). Results for other diseases are presented in the Supplemental Materials.

Discussion

In this study, we introduce a novel method for computing PRS using deep learning, employing a deep ensemble encoder-based approach that integrates autoencoders and fully connected neural networks. DEEN differentiates itself from existing PRS methods by modeling non-linear genetic effects through more flexible structures. This allows SNPs in different genomic regions to exert differential impacts on the final prediction via learned weights, unlike traditional PRS methods that apply uniform priors or regularization penalties to all SNPs. Furthermore, DEEN addresses the common issue of overfitting in deep learning models by initially employing an autoencoder model to learn a reduced latent dimension of the genetic data. Given the complexity and size of genetic datasets, directly applying a deep learning model is impractical due to computational constraints such as GPU memory limits. DEEN overcomes this by separating dimensionality reduction and final predictive modeling into distinct modules. The autoencoder module significantly reduces the correlation among input SNPs, such as those caused by LD, creating a new latent representation. This reduced input feature space allows the FCNN to build more efficient and effective predictive models of disease.

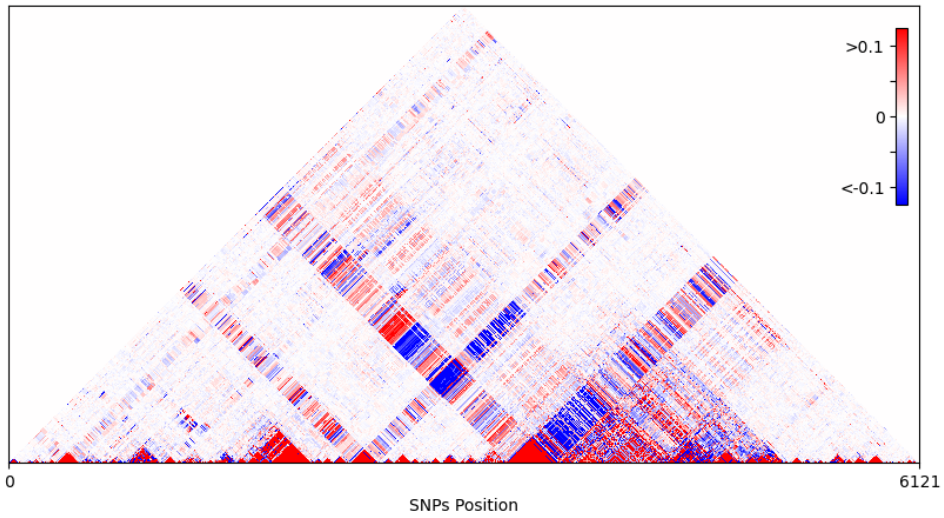

(a)

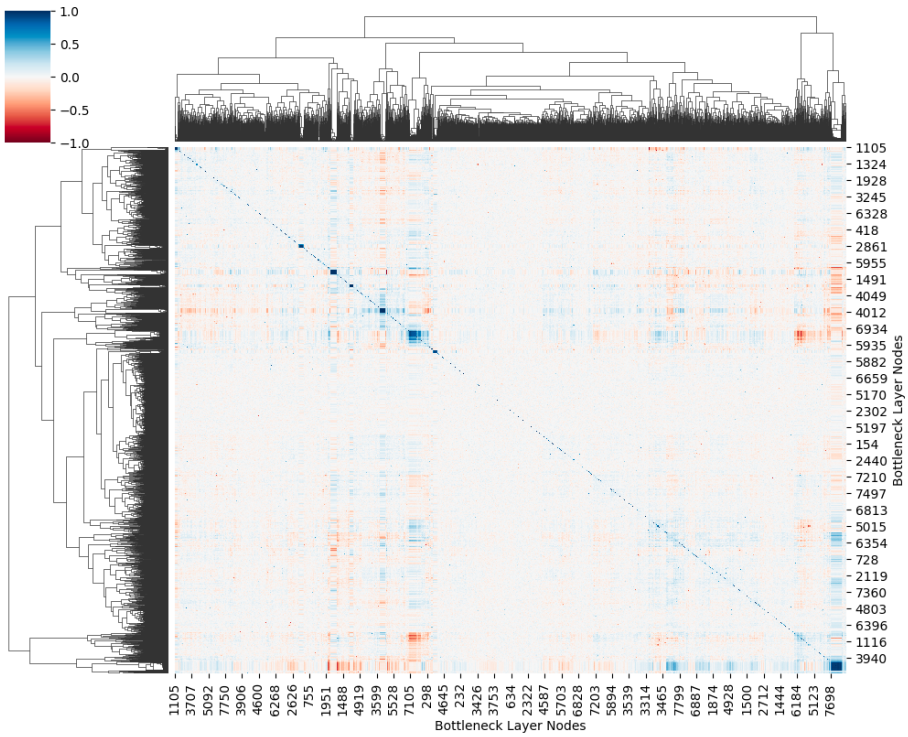

(b)

Figure 5 *Correlations in the Encoder Layer Nodes Weights and Cluster Map of Correlations in the Decoder Layer Nodes Weights. Autoencoder output from chromosome 1 in the T2D analysis is used to demonstrate the SNPs and node correlations.* ***a****. correlations of the weights of the encoder SNP inputs, calculated using the Pearson correlation coefficient. Red indicates positive correlations, while blue indicates negative correlations.* ***b****. cluster map showing the correlation values between nodes in the decoder layer of chromosome specific autoencoder. The heatmap visualizes correlations ranging from -1 to 1 representing positive correlations in red and negative correlations in blue, while white indicates no correlation.*

Through real data analysis in UKBB, we demonstrated that DEEN consistently has superior predictive performance for both binary diseases and continuous traits compared to existing PRS methods, including summary statistics PRS-CS, Lasso regression using individual-level data, and an alternative ML method, PCA-FCNN (Figure 2). In addition, risk stratification analysis, which

aligns more closely with the clinical utility of risk scores, showed that DEEN generated risk scores significantly improved our ability to identify individuals in the high-risk group (Figure 3). As individuals in the high-risk group are more likely to benefit from prevention schemes or treatment options, the proposed model is more likely to provide clinically relevant value. We also independently validated the DEEN models in the AoU dataset. Although slight performance decreases were observed due to population, demographic, and environmental differences between biobanks in different countries, the predictive performance remained higher than that of other methods.

We hypothesize that the improved predictability of DEEN is due to the disentanglement of dimensionality reduction of genetic data and predictive modeling of the outcome. Both PCA-FCNN and DEEN, which perform separate dimensionality reduction and predictive modeling, have shown better performance compared to existing PRS methods (Figure 2). On the other hand, AE has been shown to be highly efficient in extracting lower dimensions of data. Compared to dimensionality reduction using PCA, the AE model has learned a better data representation, as evidenced by the improved final prediction using the same FCNN model as the prediction module (Figures 2 and 3). When we compared the model weights of the same SNPs from the AE model and Lasso PRS, it was clear that the former model utilizes more SNPs (Figure 4). SNPs included in the DEEN model may be informative in either learning the latent representations or predicting the outcome, or both. In contrast, in Lasso PRS, SNPs that are not predictive of the outcome are removed from the model, even if they may be important in modeling the correlations among SNPs. Finally, the AE can capture both proximal and distal SNP relationships (Figure 5a). These relationships are modeled through the bottleneck layers of the AE, which has shown distinct clusters among the nodes (Figure 5b). The clustering among the bottleneck nodes indicates that different parts of the network are differentially modeling groups of SNPs. These results demonstrate that DEEN is more flexible in modeling genetic data in relation to predicting outcomes compared to existing PRS methods.

The study also has several limitations that warrant future research. The DEEN method requires individual-level genetic and phenotype data to train and optimize the model. On the other hand, the PRS-CS method only requires GWAS summary statistics to generate the PRS. As a result, DEEN is more computationally expensive than summary statistics based PRS methods, but with a gain in predictive performance. In addition, to reduce potential model overfitting and stay within the computational constraint (e.g. GPU memory), we performed the necessary variant filtering based on existing GWAS results. While the variant filtering may remove potential SNPs with small effects, the filtering was consistently applied to all methods to ensure valid comparisons. Furthermore, we evaluated multiple filtering thresholds, and the relative performances among different methods were stable. Lastly, the DEEN model may be less interpretable than PRS generated from statistical models due to the complexity of deep learning models. Developing interpretable machine learning models could potentially be incorporated into DEEN in the future.

Future research can also explore using autoencoders as a transfer learning tool to improve performance across different racial groups. Additionally, efforts can focus on improving the interpretability of autoencoder models without compromising performance, optimizing computational resources for training, and extending the application of autoencoders to other

complex diseases or datasets. Incorporating additional external validation datasets can further enhance the generalizability of our findings beyond the datasets used in the study.

In conclusion, to our knowledge, our study is the first to demonstrate the benefits of ensembling advanced machine learning algorithms, AE and FCNN, for generating improved PRS. Our study provides evidence that modeling complex genetic effects can improve the genetic risk prediction of complex diseases and traits. We also have made the DEEN algorithm publicly available on GitHub for replications and evaluations.

The Method and Data

The UKBB Dataset is a comprehensive biomedical database supporting health research in the UK and worldwide[47–50]. The data collected from more than 500,000 volunteers aged 40-69 living in the UK includes health questionnaires, electronic health records (EHR), physical measurements, biological samples, genetic information, imaging data, and digital health data. The AllofUs Dataset, which is used as external validation in this study, is a dataset containing comprehensive genetic data collected within the scope of the All of Us Research Program conducted by the US National Institutes of Health (NIH)[51]. This dataset contains the genetic data of more than 200,000 participants of different races.

Data quality control and variants selection

We performed a series of quality control (QC) measures to ensure the quality of the analyzed dataset. For sample-level QC, we retained individuals who passed the following criteria: (1). Only unrelated individuals were retained. Among related individuals, one individual from each pair was systematically removed to prevent undue influence from familial genetic connections. The threshold for relatedness was set at the level of second-degree relatives, as indicated by an identity-by-descent $\hat{\pi}$ value equal to or greater than 0.25. (2) Individuals with self-reported White British ancestry. This ensures compatibility with the population used to generate pre-trained PRS. (3) Individuals with matched self-reported and genetically inferred sexes. (4). Individuals with heterozygosity within three standard deviations from the mean. For SNP-level QC, we excluded SNPs that: (1) with more than 5% missing rate, (2) minor allele frequency of less than 1%, (3) have an imputation quality info score of less than 0.8 (4) are duplicated or ambiguous (5) Hardy-Weinberg equilibrium p-value less than 10^{-10}.

For hypertension and T2D, case and control statuses were determined using the widely adopted PheCode algorithm in UKBB, which relies on the inclusion and exclusion of disease-specific ICD-10 codes[52,53]. The continuous traits were extracted from the UKBB data fields: field 21001 for BMI, field 30690 for cholesterol, field 30760 for HDL, and field 30780 for LDL. In the All of Us data, the study cohort was created using individuals identified as White race to ensure the individuals are of similar ancestry as those in the UKBB. The phenotyping algorithms for binary diseases were obtained from PheKB[54] and implemented by the All of Us team. The corresponding continuous traits were obtained from AoU with concept ids 3038553 for BMI, 40772590 for cholesterol, 40782589 for HDL, and 40795800 for LDL. We included individuals with $13 < \text{BMI} < 42$, $25\ \text{mg/dL} < \text{Cholesterol} < 380\ \text{mg/dL}$, $1\ \text{mg/dL} < \text{HDL} < 190\ \text{mg/dL}$, and $3\ \text{mg/dL} < \text{LDL} < 270\ \text{mg/dL}$ to remove potential outliers.

In addition, when applying the proposed DEEN method, we performed variant filtering to reduce computational time and potential null signals. For each trait, we selected candidate SNPs associated with the trait using a lenient p-value threshold of less than 0.005 or 0.0005 based on GWAS results. The respective GWAS was conducted using Plink 2.0 (cite), adjusting for age, gender, ancestry principal components, and assessment center as covariates. For continuous traits, 100,000 or 150,000 SNPs with the lowest p-values were selected so that the number of SNPs was comparable to the binary diseases[55]. The entire analysis was repeated for both thresholds.

Polygenic risk score methods

The PRS-CS method is a Bayesian approach used to more accurately predict the effects of genetic variants on a set of diseases or phenotypes[26]. For our analysis, we used the following parameter settings: phi=100, n_gwas=320000. For the LD reference genome, we used the precomputed LD reference using the UK Biobank data. The phi parameter controls the global shrinkage of the effect sizes of SNPs, while n_gwas specifies the sample size of the GWAS. The GWAS summary statistics were obtained from the GWAS analysis of the UKBB[55]. Lasso (Least Absolute Shrinkage and Selection Operator) is a regression method used for variable selection and regularization, especially for high-dimensional data. We used the Lasso method implemented in the BigSNPr[46] package to generate the Lasso PRS used in this study. Specifically, we used the big_spLogReg and big_spLinReg functions for binary and continuous phenotypes, respectively. The k parameter was set to 5, representing the number of folds used in cross-validation. These parameter settings were selected using the default parameters provided by the respective methods.

Dimensionality Reduction with PCA

As a comparison to our proposed method, we also utilized a common method for dimension reduction, the principal component analysis[56] method (PCA), implemented in Sklearn[57] v1.3.1. Because PCA is an unsupervised method that does not utilize the outcome labels, we expect the dimensionality reduction to be similar across different diseases and traits. As a result, we optimized the dimension reduction using the hypertension dataset. For each chromosome, we applied PCA to reduce the dimensionality of the genetic feature space. We evaluated the PC space between 5% and 50% of the original dimensions. For each PC dimension, we calculated the variance explained and for each chromosome, we calculated the number of PCs required for the variance to exceed 90%. Since the number of PCs required varies for each chromosome, we determined the number of PCs in proportion to the number of SNPs in the chromosome. As a result of the experiments, we defined the number of PCs as the number of SNPs in the chromosome divided by 8 and determined the number of PCs required to maintain the variance at the required level. The dimension-reduced patient array for this method can be given as follows:

$$\boldsymbol{P} = pca\left(\boldsymbol{x}_{\boldsymbol{chr_1}}\right), \mathrm{pca}\left(\boldsymbol{x}_{\boldsymbol{chr_2}}\right), \ldots, \mathrm{pca}\left(\boldsymbol{x}_{\boldsymbol{chr_{22}}}\right)$$

where **x** is the input array of the chromosome. The computed patient array is then given as input to the FCNN. The modeling process of combining PCA and FCNN is referred to as PCA-FCNN in this study.

Dimensionality Reduction with Autoencoders

The proposed DEEN method consists of 3 main parts, as shown in Figure 1. In the first part, autoencoders were used for dimensionality reduction. In this study, PyTorch[58] and PyTorch Lightning[59] libraries were used to train and evaluate autoencoder and FCNN models. An autoencoder is a type of artificial neural network designed to learn efficient coding of input data through compression. It primarily consists of two components: an encoder that maps the input data to a latent space representation and a decoder that reconstructs the input data from this compressed representation. During this process, the model learns the key features of the original input. A learning process takes place to ensure that the compressed representation is as similar as possible to the original data. In this study, grid search was used for hyperparameter selection to optimize the performance of the model. Each of the hyperparameters is tested individually by trials to determine the optimal values. This manual grid search process allowed for a detailed analysis of the impact of each hyperparameter on the performance of the model and allowed for more fine-tuning.

Separate autoencoders were trained for each chromosome using the training dataset. The number of nodes in the bottleneck layer required for each chromosome was kept the same as the number of dimensions determined by the PCA experiments. The coded features of the patients in the training and test dataset were obtained using only the coder blocks of the autoencoders obtained after training. The set of hyperparameters required for training the autoencoders was the number of layers, batch size, learning rate, weight decay, activation functions, and epoch size. As AE is an unsupervised method, the optimal parameters do not depend on the outcome phenotype. As a result, these parameters were determined using only genetic data from the hypertension dataset and applied to the other diseases. MSE was used as the loss function during autoencoder training. The parameters used in the experiments for the grid search are learning rate 0.0001, 0.00001, and 0.000001, weight decay 0, 0.001, and 0.1, epoch size 100,200,400, chunk size 64,256,1024 and the number of layers 2,3 and 4. Through gird search optimization, the following parameters were determined: learning rate 0.00001, weight decay 0, epoch size 400, batch size 256, and number of layers 2. The same parameters were used for all diseases. The activation function used between the layers is ReLU[60]. Details of these experiments can be found on the GitHub page (https://github.com/okanbilge/DEEN).

The encoded chromosome is represented by a function where k is the bottleneck layer,

$$\boldsymbol{k} = \gamma(\boldsymbol{x}_{chr_t}\boldsymbol{W}_{chr_t} + \boldsymbol{b}_{chr_t})$$

where $\boldsymbol{x}_{chr_k}$ is the input matrix of the chromosome *t*, $\boldsymbol{W}_{chr_k}$ is the matrix of weights between the input and encoder layer for chromosome *t*, b is the vector of biases for the encoder layer, and $\gamma : \mathbb{R} \rightarrow \mathbb{R}$ an activation function. Similarly, the decoding network can be formulated as follows,

$$\boldsymbol{x}'_{chr_k} = \gamma'(\boldsymbol{W}'_{chr_t}\boldsymbol{k} + \boldsymbol{b}_{chr_t}{}')$$

where $\boldsymbol{W}'_{chr_t}$ is the weight matrix between the encoder and output layer of the autoencoder. The loss function for each chromosome is given as:

$$argmin\left(L\left(\left(\boldsymbol{x}'_{\boldsymbol{chr_t}}, \boldsymbol{x}_{\boldsymbol{chr_t}}\right)\right)\right)$$

where L is the loss function. We can write the resulting loss function with MSE as follows:

$$argmin\left((\gamma'(\boldsymbol{W'}_{\boldsymbol{chr_t}}\boldsymbol{k} + \boldsymbol{b}_{\boldsymbol{chr_t}}') - \gamma(\boldsymbol{x}_{\boldsymbol{chr_t}}\boldsymbol{W}_{\boldsymbol{chr_t}} + \boldsymbol{b}_{\boldsymbol{chr_t}}))^2\right)$$

After this minimization process, Patient array P is calculated using the calculated weights as follows:

$$\boldsymbol{P} = \gamma(\boldsymbol{x}_{\boldsymbol{chr_1}}\boldsymbol{W}_{\boldsymbol{chr_1}} + \boldsymbol{b}_{\boldsymbol{chr_1}}), \gamma(\boldsymbol{x}_{\boldsymbol{chr_2}}\boldsymbol{W}_{\boldsymbol{chr_2}} + \boldsymbol{b}_{\boldsymbol{chr_2}}), \dots, \gamma(\boldsymbol{x}_{\boldsymbol{chr_22}}\boldsymbol{W}_{\boldsymbol{chr_22}} + \boldsymbol{b}_{\boldsymbol{chr_{22}}})$$

The computed patient array is then given as input to the FCNN.

Fully Connected Neural Networks

Fully Connected Neural Networks (FCNN) is a widely used model in artificial neural networks. FCNN consists of layers where each neuron is connected to all neurons in the previous layer. These networks usually operate as feedforward networks, meaning that information flows unidirectionally from the input layer of the network to the output layer. After dimensionality reduction in both PCA-FCNN and autoencoder-based methods, the reduced data was used for classification or regression with FCNN. The hyperparameter optimization for this method was similar to the autoencoder method. The set of hyperparameters required to train the FCNN is the number of layers, node size, batch size, learning rate, weight decay, activation functions, and epoch size. These hyperparameters were determined by conducting separate training for each phenotype. As with the autoencoder method, a manual grid search was performed on pre-defined values to obtain the best results. These experiments were carried out using several network models with 2,3, and 4 layers and sizes ranging from 16 to 2048 with learning rates 0.0001 and 0.00001, weight decay 0, 0.001, and 0.1, and batch sizes 256-512-1024.

This patient array will be used as input to the first hidden layer of the classification/regression network:

$$h^{(1)} = \gamma(\boldsymbol{W}^{(1)}(\boldsymbol{P}) + \boldsymbol{b}^{(1)}$$

Between hidden layers:

$$h^{(i)} = \gamma(\boldsymbol{W}^{(i)}h^{(i-1)}) + \boldsymbol{b}^{(1)}$$

Between the last hidden layer to the classification layer:

$$\hat{y} = \boldsymbol{W}^{(L)}h^{(L-1)} + \boldsymbol{b}^{(L)}$$

where L is the decision layer, and i is the layer number of the classification/regression network.

Binary Cross Entropy(CE) was used as the loss function in the classification models, while MSE was used in the regression models. The formulation of MSE and BCE were given as,

$$MSE = \frac{1}{n}\sum_{i=1}^{n}(y_i - \hat{y}_i)^2$$

$$BCE = \frac{1}{n}\sum_{i=1}^{n}(y_i \log(\hat{y}_i) + (1 - y_i)\log(1 - \hat{y}_i))$$

where y_i is the observed value of the patient *i*, $\hat{y}_i$ is the estimated value of the patient *i*, and n is the number of patients.

Correlation Analysis with Autoencoders

Autoencoders can identify important patterns among SNPs and generate a lower-dimensional encoding (latent space) representation of these SNPs. During the learning process, each input SNP is connected to neurons in the hidden layer of the model through learned weights. These weights determine how the model processes the input data and highlight the importance of each SNP. By analyzing the correlation of these weights, we can identify associations between different input SNPs. E.g. a high correlation between the weights of two SNPs may suggest that they contribute similarly to the model. In this study, we examined the correlation between the weights of the autoencoders trained separately for each chromosome to investigate correlative relationships among SNPs. These relationships can indicate potential linear or non-linear interactions that are important for learning the latent representation. Conversely, analyzing correlations between nodes in the bottleneck layers can reveal nodes that differentially model groups of SNPs. Such correlations could indicate that the model captures the finer and more complex structure of the data.

Methods evaluations

To accurately assess the performance of the proposed model, we applied 5-fold cross-validation to the UKBB data, where the dataset was divided into five equal parts. Each part was used as the testing data once, while the remaining four parts were used as the training data. This process was repeated five times. The performance of the model was evaluated for all 5 testing splits. Subsequently, the same models trained on the UKBB dataset were applied to the AuO dataset for independent external evaluations.

The study used two performance metrics, MSE for continuous traits and AUC (Area Under the Curve) for binary diseases for evaluating the predictive performances of PRS models. MSE is a commonly used error measure in regression problems. It is calculated by averaging the square of the differences between actual and predicted values. A lower MSE indicates better performance of the model. AUC refers to the area under the Receiver Operating Characteristics (ROC) curve, which plots the True Positive Rate (TPR) against the False Positive Rate (FPR) at various thresholds. TPR (True Positive Rate) measures the proportion of actual positive cases that are correctly identified by the model, while FPR (False Positive Rate) measures the proportion of actual negative cases that are incorrectly classified as positive by the model. AUC takes a value between 0 and 1, with a value closer to 1 indicating better classification ability of the model.

To assess the risk stratification of PRS models, we calculated the odds ratio of case enrichment between high-risk and low-risk individuals. We stratified individuals into high-risk and low-risk groups based on their predicted probabilities. For the low-risk group, we selected individuals with the lowest 5% predicted probabilities according to each model. Conversely, we

varied the high-risk group selection for each model by progressively relaxing the predicted probability threshold from the top 5% to the top 25%, in increments of 5%. A logistic regression model was then employed to determine the odds ratio enrichment of cases between the high-risk and low-risk groups for each model at each threshold.

The development and training of deep learning models was carried out using the PyTorch and PyTorchLightning libraries. In the training process, we used a hardware configuration with a 32-core CPU, 1 NVIDIA A100 GPU, and 100 GB RAM.

Data availability

The UKBB is a large-scale biomedical database with genetic and health information from more than 500,000 UK participants. Available for research by request at https://www.ukbiobank.ac.uk. The UKBB data was approved under application # 86494 The All of Us Research Program is a large-scale biomedical database with diverse health data from over one million U.S. participants. Available for research by request at this link: https://www.researchallofus.org/

Code availability

We provide the scripts used to perform the model training and inference proposed in the article in the GitHub repository https://github.com/okanbilge/DEEN

Acknowledgments

"The All of Us Research Program is supported by the National Institutes of Health, Office of the Director: Regional Medical Centers: 1 OT2 OD026549; 1 OT2 OD026554; 1 OT2 OD026557; 1 OT2 OD026556; 1 OT2 OD026550; 1 OT2 OD 026552; 1 OT2 OD026553; 1 OT2 OD026548; 1 OT2 OD026551; 1 OT2 OD026555; IAA #: AOD 16037; Federally Qualified Health Centers: HHSN 263201600085U; Data and Research Center: 5 U2C OD023196; Biobank: 1 U24 OD023121; The Participant Center: U24 OD023176; Participant Technology Systems Center: 1 U24 OD023163; Communications and Engagement: 3 OT2 OD023205; 3 OT2 OD023206; and Community Partners: 1 OT2 OD025277; 3 OT2 OD025315; 1 OT2 OD025337; 1 OT2 OD025276. In addition, the All of Us Research Program would not be possible without the partnership of its participants."

R.L is supported in part by Cedars Sinai Department of Neurology/Jona Goldrich Center for Alzheimer's & Memory Disorders. O.B.O, R.C, and R.L are supported by the Department of Computational Biomedicine, Cedars Sinai.

Author Contributions

O.B.O. and R.L. contributed to method development, model training, and writing the paper, while R.C. contributed to data processing.

References

1. Klarin, D. & Natarajan, P. Clinical utility of polygenic risk scores for coronary artery disease. *Nat Rev Cardiol* **19**, 291–301 (2022).
2. Lee, J. J. *et al.* Gene discovery and polygenic prediction from a genome-wide association study of educational attainment in 1.1 million individuals. *Nat Genet* **50**, 1112–1121 (2018).
3. Jansen, P. R. *et al.* Genome-wide analysis of insomnia in 1,331,010 individuals identifies new risk loci and functional pathways. *Nat Genet* **51**, 394–403 (2019).
4. Watanabe, K. *et al.* A global overview of pleiotropy and genetic architecture in complex traits. *Nat Genet* **51**, 1339–1348 (2019).
5. Abdellaoui, A., Yengo, L., Verweij, K. J. H. & Visscher, P. M. 15 years of GWAS discovery: realizing the promise. *The American Journal of Human Genetics* **110**, 179–194 (2023).
6. Sollis, E. *et al.* The NHGRI-EBI GWAS Catalog: knowledgebase and deposition resource. *Nucleic Acids Res* **51**, D977–D985 (2023).
7. Ku, C. S., Loy, E. Y., Pawitan, Y. & Chia, K. S. The pursuit of genome-wide association studies: where are we now? *J Hum Genet* **55**, 195–206 (2010).
8. Wang, Q. *et al.* Rare variant contribution to human disease in 281,104 UK Biobank exomes. *Nature* **597**, 527–532 (2021).
9. Corvol, H. *et al.* Genome-wide association meta-analysis identifies five modifier loci of lung disease severity in cystic fibrosis. *Nat Commun* **6**, 8382 (2015).
10. Elliott, L. T. *et al.* Genome-wide association studies of brain imaging phenotypes in UK Biobank. *Nature* **562**, 210–216 (2018).
11. Hill, W. D. *et al.* Genome-wide analysis identifies molecular systems and 149 genetic loci associated with income. *Nat Commun* **10**, 5741 (2019).
12. Torkamani, A., Wineinger, N. E. & Topol, E. J. The personal and clinical utility of polygenic risk scores. *Nat Rev Genet* **19**, 581–590 (2018).
13. Thomas, M. *et al.* Genome-wide modeling of polygenic risk score in colorectal cancer risk. *The American journal of human genetics* **107**, 432–444 (2020).
14. Denny, J. C., Bastarache, L. & Roden, D. M. Phenome-wide association studies as a tool to advance precision medicine. *Annu Rev Genomics Hum Genet* **17**, 353–373 (2016).
15. Euesden, J., Lewis, C. M. & O'reilly, P. F. PRSice: polygenic risk score software. *Bioinformatics* **31**, 1466–1468 (2015).
16. Raychaudhuri, S. *et al.* Identifying relationships among genomic disease regions: predicting genes at pathogenic SNP associations and rare deletions. *PLoS Genet* **5**, e1000534 (2009).
17. Chatterjee, N., Shi, J. & Garc\'\ia-Closas, M. Developing and evaluating polygenic risk prediction models for stratified disease prevention. *Nat Rev Genet* **17**, 392–406 (2016).
18. Kachuri, L. *et al.* Principles and methods for transferring polygenic risk scores across global populations. *Nat Rev Genet* **25**, 8–25 (2024).
19. Farooqi, R., Kooner, J. S. & Zhang, W. Associations between polygenic risk score and covid-19 susceptibility and severity across ethnic groups: UK Biobank analysis. *BMC Med Genomics* **16**, 150 (2023).

20. Khera, A. V *et al.* Genome-wide polygenic scores for common diseases identify individuals with risk equivalent to monogenic mutations. *Nat Genet* **50**, 1219–1224 (2018).
21. Truong, B. *et al.* Integrative polygenic risk score improves the prediction accuracy of complex traits and diseases. *Cell Genomics* **4**, (2024).
22. Purcell, S. M. *et al.* Common polygenic variation contributes to risk of schizophrenia and bipolar disorder. *Nature* **460**, 748–752 (2009).
23. Chen, J. *et al.* Pruning and thresholding approach for methylation risk scores in multi-ancestry populations. *Epigenetics* **18**, 2187172 (2023).
24. Liu, W., Zhuang, Z., Wang, W., Huang, T. & Liu, Z. An improved genome-wide polygenic score model for predicting the risk of type 2 diabetes. *Front Genet* **12**, 632385 (2021).
25. Mak, T. S. H., Porsch, R. M., Choi, S. W., Zhou, X. & Sham, P. C. Polygenic scores via penalized regression on summary statistics. *Genet Epidemiol* **41**, 469–480 (2017).
26. Ge, T., Chen, C.-Y., Ni, Y., Feng, Y.-C. A. & Smoller, J. W. Polygenic prediction via Bayesian regression and continuous shrinkage priors. *Nat Commun* **10**, 1776 (2019).
27. Privé, F., Arbel, J. & Vilhjálmsson, B. J. LDpred2: better, faster, stronger. *Bioinformatics* **36**, 5424–5431 (2020).
28. Vilhjálmsson, B. J. *et al.* Modeling linkage disequilibrium increases accuracy of polygenic risk scores. *The american journal of human genetics* **97**, 576–592 (2015).
29. Albiñana, C. *et al.* Multi-PGS enhances polygenic prediction by combining 937 polygenic scores. *Nat Commun* **14**, 4702 (2023).
30. Lee, A., Caron, F., Doucet, A. & Holmes, C. Bayesian sparsity-path-analysis of genetic association signal using generalized t priors. *Stat Appl Genet Mol Biol* **11**, (2012).
31. Hemani, G. *et al.* Retracted article: Detection and replication of epistasis influencing transcription in humans. *Nature* **508**, 249–253 (2014).
32. Elgart, M. *et al.* Non-linear machine learning models incorporating SNPs and PRS improve polygenic prediction in diverse human populations. *Commun Biol* **5**, 856 (2022).
33. Yu, S. & Principe, J. C. Understanding autoencoders with information theoretic concepts. *Neural Networks* **117**, 104–123 (2019).
34. Bank, D., Koenigstein, N. & Giryes, R. Autoencoders. *Machine learning for data science handbook: data mining and knowledge discovery handbook* 353–374 (2023).
35. Chen, S. & Guo, W. Auto-encoders in deep learning—a review with new perspectives. *Mathematics* **11**, 1777 (2023).
36. Pinaya, W. H. L., Vieira, S., Garcia-Dias, R. & Mechelli, A. Autoencoders. in *Machine learning* 193–208 (Elsevier, 2020).
37. Shankar, V. & Parsana, S. An overview and empirical comparison of natural language processing (NLP) models and an introduction to and empirical application of autoencoder models in marketing. *J Acad Mark Sci* **50**, 1324–1350 (2022).
38. Murtagh, F. Multilayer perceptrons for classification and regression. *Neurocomputing* **2**, 183–197 (1991).
39. Svozil, D., Kvasnicka, V. & Pospichal, J. Introduction to multi-layer feed-forward neural networks. *Chemometrics and intelligent laboratory systems* **39**, 43–62 (1997).
40. Rocha, M., Cortez, P. & Neves, J. Evolution of neural networks for classification and regression. *Neurocomputing* **70**, 2809–2816 (2007).

41. Kang, K. & Wang, X. Fully convolutional neural networks for crowd segmentation. *arXiv preprint arXiv:1411.4464* (2014).
42. Sigurdsson, A. I. *et al.* Deep integrative models for large-scale human genomics. *Nucleic Acids Res* **51**, e67–e67 (2023).
43. Xu, Y. *et al.* Machine learning optimized polygenic scores for blood cell traits identify sex-specific trajectories and genetic correlations with disease. *Cell Genomics* **2**, (2022).
44. Taş, G. *et al.* Computing linkage disequilibrium aware genome embeddings using autoencoders. *Bioinformatics* btae326 (2024).
45. Bycroft, C. *et al.* The UK Biobank resource with deep phenotyping and genomic data. *Nature* **562**, 203–209 (2018).
46. Privé, F., Aschard, H., Ziyatdinov, A. & Blum, M. G. B. Efficient analysis of large-scale genome-wide data with two R packages: bigstatsr and bigsnpr. *Bioinformatics* **34**, 2781–2787 (2018).
47. Sudlow, C. *et al.* UK biobank: an open access resource for identifying the causes of a wide range of complex diseases of middle and old age. *PLoS Med* **12**, e1001779 (2015).
48. Littlejohns, T. J., Sudlow, C., Allen, N. E. & Collins, R. UK Biobank: opportunities for cardiovascular research. *Eur Heart J* **40**, 1158–1166 (2019).
49. Canela-Xandri, O., Rawlik, K. & Tenesa, A. An atlas of genetic associations in UK Biobank. *Nat Genet* **50**, 1593–1599 (2018).
50. Fry, A. *et al.* Comparison of sociodemographic and health-related characteristics of UK Biobank participants with those of the general population. *Am J Epidemiol* **186**, 1026–1034 (2017).
51. All of Us Research Program Investigators, A. The “All of Us” research program. *New England Journal of Medicine* **381**, 668–676 (2019).
52. Wei, W.-Q. *et al.* Evaluating phecodes, clinical classification software, and ICD-9-CM codes for phenome-wide association studies in the electronic health record. *PLoS One* **12**, e0175508 (2017).
53. Wu, P. *et al.* Mapping ICD-10 and ICD-10-CM codes to phecodes: workflow development and initial evaluation. *JMIR Med Inform* **7**, e14325 (2019).
54. Kirby, J. C. *et al.* PheKB: a catalog and workflow for creating electronic phenotype algorithms for transportability. *Journal of the American Medical Informatics Association* **23**, 1046–1052 (2016).
55. Walters, R. & Palmer, D. Nealelab/UKBB_ldsc: v2.0.0 (Round 2 GWAS update). Preprint at https://doi.org/10.5281/zenodo.7186871 (2022).
56. Abdi, H. & Williams, L. J. Principal component analysis. *Wiley Interdiscip Rev Comput Stat* **2**, 433–459 (2010).
57. Pedregosa, F. Scikit-learn: Machine learning in python. *Journal of machine learning research* **12**, 2825 (2011).
58. Paszke, A. *et al.* Pytorch: An imperative style, high-performance deep learning library. *Adv Neural Inf Process Syst* **32**, (2019).
59. Falcon, W. *et al.* PyTorchLightning/pytorch-lightning: 0.7. 6 release. *Zenodo* (2020).
60. Agarap, A. F. Deep learning using rectified linear units (relu). *arXiv preprint arXiv:1803.08375* (2018).